JOURNAL OF COMPUTATIONAL PHYSICS 33, 301–312 (1979)

A Primitive Variable Finite Element Formulation for Inviscid, Compressible Flow

CLIVE A. J. FLETCHER

Department of Mechanical Engineering, University of Sydney, N.S.W. 2006, Australia

Received May 17, 1978; revised November 29, 1978

A primitive variable, least-squares finite element formulation for inviscid, compressible flow is proposed. A unique feature of the formulation is the representation of groups of variables rather than single variables. Numerical solutions are presented for two-dimensional, subcritical flow about circular and elliptic cylinders and two representative airfoils.

1. INTRODUCTION

Finite element methods have been applied to flow problems with the greatest success when the governing equations are elliptic in character. In particular, viscous, incompressible flow has received considerable attention, e.g., [1–3]. The early finite element formulations [1] were based on a variational principle applied to the Navier–Stokes equations in streamfunction/vorticity variables. Recent applications [2, 3] have more often used a Galerkin formulation in conjunction with the Navier–Stokes equations written in primitive variables. Subsonic, inviscid flow is also governed by equations that are elliptic in character. By recasting the governing equations into a streamfunction or velocity potential form, it is straightforward to derive a related variational principle. Previous finite element treatments of this problem have been based on such a variational principle, e.g., [4–6].

If finite element formulations for subsonic, inviscid flow are to be extended to handle transonic, inviscid flow, then the formulation must handle correctly the small regions in the flow where the governing equations are hyperbolic. An attempt to formulate a variational principle that is valid for transonic flow has been made [7], although no results were presented. Since a variational formulation can always be rewritten as a Galerkin formulation and since a conventional Galerkin formulation preserves the elliptic character of the original equations, it seems unlikely that a variational formulation will produce solutions to the transonic flow problem that exhibit evidence of a supersonic region terminated by an internal shock.

Because of the unsuitability of a variational approach to the transonic flow problem and because of the computational disadvantages (to be discussed below) of casting the governing equations in a velocity potential or streamfunction form, the present approach is based on the governing equations for the primitive variables in conservation form. An analytic representation is made for groups of variables that appear in

0021-9991/79/120301-12$02.00/0

the governing equation rather than for single variables. A least-squares formulation is applied to the resulting equation residuals and solutions are presented for subcritical, two-dimensional flow about circular and elliptic cylinders and for the flow about a 6% circular-arc airfoil and an NACA-0012 airfoil. A generalization of the least-least-squares formulation, that will permit the method to be extended to handle correctly transonic flow in which shocks would be expected, will be described in a later paper.

The governing equations for two-dimensional, subcritical, inviscid flow, in terms of the velocity potential, ϕ, are

$$(a^2 - \phi_x^2) \cdot \phi_{xx} - 2 \cdot \phi_x \cdot \phi_y \cdot \phi_{xy} + (a^2 - \phi_y^2) \cdot \phi_{yy} = 0 \tag{1}$$

and

$$a^2 + \frac{\gamma - 1}{2} \cdot (\phi_x^2 + \phi_y^2) = a_0^2, \tag{2}$$

where a is the sound speed, a_0 is the stagnation sound speed, and γ is the specific heat ratio. A finite element formulation based on the above equation has the advantage that only one unknown, $\bar{\phi}_j$, is required at each node. Equation (2) is a local algebraic relationship which updates the value of "a" at each step of the iteration.

Equation (1) can be rewritten as a Poisson-like equation

$$\phi_{xx} + \phi_{yy} = f \tag{3}$$

in which f includes all the terms that account for the compressible nature of the flow. Application of a variational finite element formulation to Eq. (3) permits an iterative procedure to be employed in which f is updated after each solution for $\bar{\phi}_j$. The iterative procedure becomes less efficient as Mach number increases and fails for a local Mach number just above 1.00 [6]. In practical problems, the pressure at the body surface is often required. To obtain the pressure from the final solution of the velocity potential, a numerical differentiation is required. The form of f, in Eq. (3), is such that a large number of cross terms must be evaluated and manipulated at each step of the iterative process; this is computationally inefficient.

To avoid the above difficulties and to permit extension into the transonic flow regime, a primitive variable formulation is proposed. The governing equations in conservation form are

$$(\rho u)_x + (\rho v)_y = 0, \tag{4}$$

$$(\rho u^2 + p)_x + (\rho uv)_y = 0, \tag{5}$$

$$(\rho uv)_x + (\rho v^2 + p)_y = 0, \tag{6}$$

and

$$p = k \cdot \rho^\gamma. \tag{7}$$

The following nondimensionalization is introduced,

$$u_{nd} = u/U_\infty \quad v_{nd} = v/U_\infty \quad \rho_{nd} = \rho/\rho_\infty\,, \qquad \text{and} \qquad p_{nd} = (p - p_\infty)/\rho U_\infty{}^2.$$

Substitution of the above into Eqs. (4–6) produces no change in appearance if the subscript *nd* is dropped. Equation (7) is replaced by

$$1 + \gamma \cdot M_\infty{}^2 \cdot p = \rho^\gamma. \tag{8}$$

The far-field boundary conditions have been applied at a finite distance from the body in the form

$$\begin{aligned} u &= u_{ff}\,, \\ v &= v_{ff}\,, \\ \rho &= \rho_{ff}\,. \end{aligned} \tag{9}$$

To obtain u_{ff}, v_{ff}, and ρ_{ff} a Prandtl–Glauert coordinate transformation has been applied in conjunction with either complex variable theory or thin airfoil theory; details are indicated in [8]. The boundary condition at the body surface requires that there is no flow through the body surface. A typical flow-field geometry for the flow about a circular cylinder is shown in Fig. 1. Symmetry about AC is imposed by requiring that $v = 0$ on AB and CD.

2. Finite Element Formulation

Equations (4)–(6) all have the same linear form, i.e.,

$$\frac{\partial F}{\partial x} + \frac{\partial G}{\partial y} = 0. \tag{10}$$

The introduction of a conventional finite element analytic representation, e.g.

$$\begin{aligned} u &= \sum_j N_j(x, y) \cdot \overline{u_j}\,, \\ v &= \sum_j N_j(x, y) \cdot \overline{v_j}\,, \qquad \text{etc.}, \end{aligned} \tag{11}$$

would destroy the similarity of form. Therefore, in the present formulation, representations for groups of variables are introduced, e.g.,

$$\begin{aligned} \rho u &= \sum_j N_j(x, y) \cdot \overline{\rho u_j}\,, \\ \rho u v &= \sum_j M_j(x, y) \cdot \overline{\rho u v_j}\,, \qquad \text{etc.}, \end{aligned} \tag{12}$$

where M_j and N_j are finite element shape functions of, as yet, undetermined order and the overbar indicates the nodal value. The technique of representing groups of variables rather than single variables has been used before in applying the orthonormal method of integral relations to supersonic boundary layer flow [9, 10]. However this is the first time such a technique has been used in a finite element application, although the same concept has been suggested in a finite difference context [11]. Representing groups of variables retains the linearity of the equations and permits a lower-order numerical integration scheme to be employed. Since only single summa-

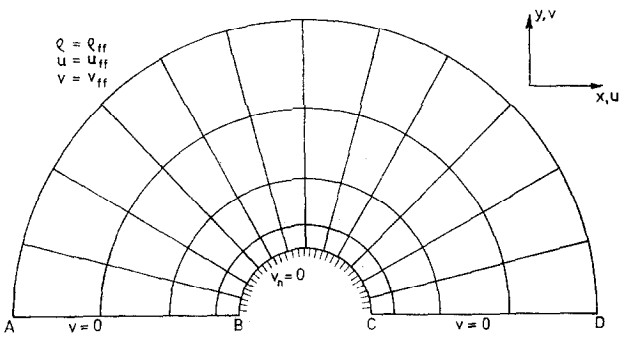

FIG. 1. Schematic of grid for circular and elliptic cylinders.

tions appear (compared with triple summations for a conventional finite element formulation) less algebraic effort and computation time is required to produce the algebraic equations.

To produce accurate computational results it is important that the order of representation of the unknowns in Eq. (12) is chosen consistently. For slow viscous flow (low Reynolds number) the dominant terms in the momentum equations are the pressure gradient term and the viscous dissipation term. If these two terms are to produce a consistent error it is necessary to adopt a representation for pressure that is one order lower than that for velocity. Typically [2, 3] the pressure variation is represented by a first-order polynomial and the velocity variation by a second-order polynomial. If the Reynolds number is not small then the dominant terms in the momentum equations are the inertia terms and the pressure gradient terms except where close to the body surface. To consistently represent this physical balance the pressure interpolation should be second order if the velocity interpolation is first order.

Olson and Tuann have carried out an eigenvalue analysis of various formulations of the incompressible Navier–Stokes equations that indicates the pressure interpolation should be one order less than the velocity interpolation irrespective of the Reynolds number. If this is correct it implies that a finite element solution in primitive variables at moderate Reynolds number will not produce very accurate solutions for the pressure. An alternative interpretation of the eigenvalue analysis is that the lower-order

pressure representation is a consequence and hence a disadvantage of the variational formulation in primitive variables.

For the present problem all terms in each equation are expected to be of equal magnitude. Since only first derivatives appear, each term will contribute equally to the order of magnitude of the equation residual. Hence,

$$\frac{O(M_j)}{O(N_j)} = \frac{2\gamma}{\gamma + 1}. \tag{13}$$

Since only integer order representations are possible the lowest consistent representation, with $\gamma = 1.4$, would have N_j as a sixth-order shape function and M_j as a seventh-order shape function. Using such high-order representations would be unwieldy and due to the relatively dense stiffness matrix might well be inefficient. Consequently in the present formulation M_j and N_j have been taken to be of the same order; based on the results of [13] quadratic, rectangular serendipity elements have been used for all groups of variables.

It is interesting, in the light of [12], that attempts to apply the above representation with a Galerkin formulation led to a singular Jacobian when used with Newton's method [8] which could only be avoided by using the Bernoulli equation on the y-axis of symmetry and the body surface. When the quadratic representation was used with a least-squares formulation the Jacobian was well behaved.

Substitution of representations like Eq. (12) into Eqs. (4)–(6) produces the following residuals

$$R^{(1)} = \sum_j \frac{\partial N_j}{\partial x} \cdot (\overline{\rho u})_j + \sum_j \frac{\partial N_j}{\partial y} \cdot (\overline{\rho v})_j, \tag{14}$$

$$R^{(2)} = \sum_j \frac{\partial N_j}{\partial x} \cdot (\overline{\rho u^2} + \bar{p})_j + \sum_j \frac{\partial N_j}{\partial y} \cdot (\overline{\rho uv})_j, \tag{15}$$

$$R^{(3)} = \sum_j \frac{\partial N_j}{\partial x} \cdot (\overline{\rho uv})_j + \sum_j \frac{\partial N_j}{\partial y} \cdot (\overline{\rho v^2} + \bar{p})_j. \tag{16}$$

The least-squares formulation requires that

$$\iint (\alpha_1 \cdot R^{(1)2} + \alpha_2 \cdot R^{(2)2} + \alpha_3 \cdot R^{(3)2})\, dx\, dy = \text{minimum}, \tag{17}$$

where α_1, α_2, and α_3 are scalars that may be used to adjust the relative weight of the various residuals. For all the results presented $\alpha_1 = \alpha_2 = \alpha_3 = 1$. Differentiating Eq. (17) with respect to the unknown nodal values gives

$$\iint \left\{\alpha_1 \cdot \frac{\partial R^{(1)}}{\partial \bar{q}_i} \cdot R^{(1)} + \alpha_2 \cdot \frac{\partial R^{(2)}}{\partial \bar{q}_i} \cdot R^{(2)} + \alpha_3 \cdot \frac{\partial R^{(3)}}{\partial \bar{q}_i} \cdot R^{(3)}\right\} dx\, dy = 0, \qquad i = 1, n, \tag{18}$$

where $\bar{q}_i = \{(\overline{\rho u})_i, (\overline{\rho v})_i, \bar{p}_i\}$. Substitution of Eqs. (14)–(16) and evaluation of the integrals produces an algebraic equation of the following form:

$$S_i^{(m)} = \sum_j \{r_{ij}^{(m)} \cdot (\overline{\rho u})_j + s_{ij}^{(m)} \cdot (\overline{\rho v})_j + t_{ij}^{(m)} \cdot (\overline{\rho u^2})_j + x_{ij}^{(m)} \cdot (\overline{\rho uv})_j$$

$$+ y_{ij}^{(m)} \cdot (\overline{\rho v^2})_j + z_{ij}^{(m)} \cdot \bar{p}_j\} = 0, \qquad m = 1, 3, \quad i = 1, n. \tag{19}$$

In Eq. (19), $m = 1$ corresponds to $\bar{q}_i = (\overline{\rho u})_i$ in Eq. (18). Thus for the three nodal unknowns $(\overline{\rho u}_i, \overline{\rho v}_i, \bar{p}_i)$, three equations are formed. In Eq. (19), $r_{ij}^{(m)}$, etc., are algebraic functions of $a_{ij}, b_{ij}, c_{ij}, d_{ij}, \overline{\rho u}_i, \overline{\rho v}_i$, and $\bar{p}_i$ where

$$\begin{aligned} a_{ij} &= \iint \frac{\partial N_i}{\partial x} \cdot \frac{\partial N_j}{\partial x} \cdot dx\, dy, \\ b_{ij} &= \iint \frac{\partial N_i}{\partial y} \cdot \frac{\partial N_j}{\partial y} \cdot dx\, dy, \\ c_{ij} &= \iint \frac{\partial N_i}{\partial x} \cdot \frac{\partial N_j}{\partial y} \cdot dx\, dy, \\ d_{ij} &= \iint \frac{\partial N_i}{\partial y} \cdot \frac{\partial N_j}{\partial x} \cdot dx\, dy. \end{aligned} \tag{20}$$

Equations (20) are evaluated numerically in the (ξ, η) plane; an isoparametric mapping [13] connects the physical (x, y) plane to the (ξ, η) plane. The algebraic expressions for $r_{ij}^{(m)}$, etc., are given in the Appendix.

3. Iterative Solution Techniques

The least-squares formulation has the advantage of producing a diagonally dominant stiffness matrix. Consequently, an iterative algorithm of the relaxation type is possible. By considering the dependence of $S_i^{(m)}$, in Eq. (19), on the diagonal term it is possible to write down the following iterative scheme

$$q_i^{\nu+1} = q_i^{\nu} - \lambda \cdot \left[\frac{\partial S_i^{(m)}}{\partial q_i}(\bar{q}_\nu)\right]^{-1} \cdot S_i^{(m)}(\bar{q}_\nu). \tag{21}$$

The symbol ν is the iteration step and λ is a scalar that is chosen to increase the rate of convergence. The iterative process was convergent if λ was not greater than 1.7. The algorithm has the advantage of converging from any starting value and requiring relatively little storage since $[\partial S_i^{(m)}/\partial q_i]$ is a scalar and trivial to invert. However the iterative scheme was rather slow; the results for the NACA-0012 airfoil presented in Section 4 typically took 4–5 min of CPU time on an IBM 370/168 to converge.

Equation (19) has also been solved using Newton's method. In this case the iterative scheme is

$$\bar{q}_i^{\nu+1} = \bar{q}_i^{\nu} - [J_\nu]^{-1} \cdot S_i^{(m)}(\bar{q}_i), \tag{22}$$

where J_ν is the Jacobian, $\partial S_i^{(m)}/\partial \bar{q}$. The factorization of the Jacobian required considerable storage and execution time even though sparse matrix techniques were used [13]. Newton's method was also used with a Galerkin formulation [13] and considerable difficulty was experienced with the reduction in radius of convergence as the number of unknowns, n, increased [14].

For the flow about a 6% circular-arc airfoil with a coarse grid (90 nodal unknowns) Newton's method was about four times as fast as the relaxation method. However it was necessary to apply the relaxation method for 10 steps to provide suitable starting data for Newton's method.

4. Results

Numerical solutions are presented for the compressible flow past circular and elliptic cylinders and two representative airfoils at zero angle of attack. All the results presented are for subcritical flow and were obtained with the relaxation method described above.

A schematic of the finite element grid for the flow about circular and elliptic cylinders is shown in Fig. 1. An isoparametric mapping relates the polar coordinates to the Cartesian coordinates in which the equation are written. For these two examples there are two stagnation points on the body at which the velocity components, u and

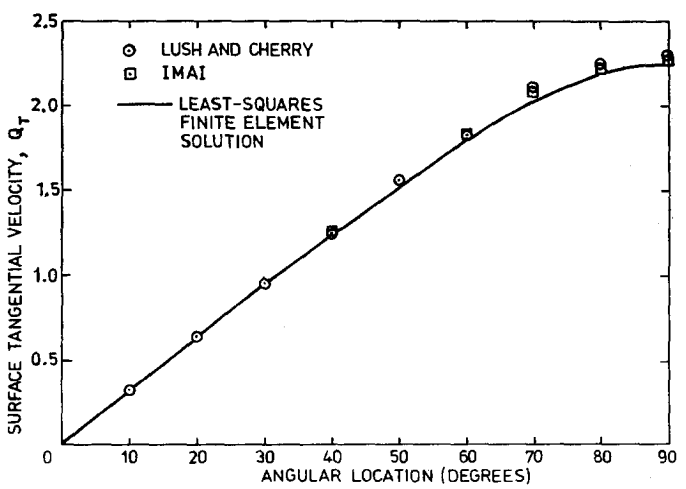

FIG. 2. Surface velocity variation for the flow about a circular cylinder at $M_\infty = 0.40$.

v, are zero. In the present formulation the pressure and density at the stagnation points are considered part of the boundary conditions. If the Bernoulli equation is combined with Eq. (8), the following expressions are obtained for the stagnation values of density and pressure,

$$\rho_{sp} = \left\{1 + \left(\frac{\gamma - 1}{2}\right) M_\infty^2\right\}^{1/(\gamma-1)}, \tag{23}$$

and

$$p_{sp} = (\rho_{sp}^\gamma - 1)/\gamma M_\infty^2. \tag{24}$$

Numerical results for the flow about a circular cylinder with a freestream Mach number of 0.4 are presented in Fig. 2. The finite element solution was obtained with 91 elements and 829 nodal unknowns. The finite element results are seen to be in good agreement with the series solutions of Imai [15] and Lush and Cherry [16]. The finite element solution indicated that the flow was just sonic at the shoulder of the circular cylinder.

Numerical solutions for the flow about a 2 : 1 elliptic cylinder at a freestream Mach number of 0.5 are shown in Fig. 3. These results were obtained with 91 elements

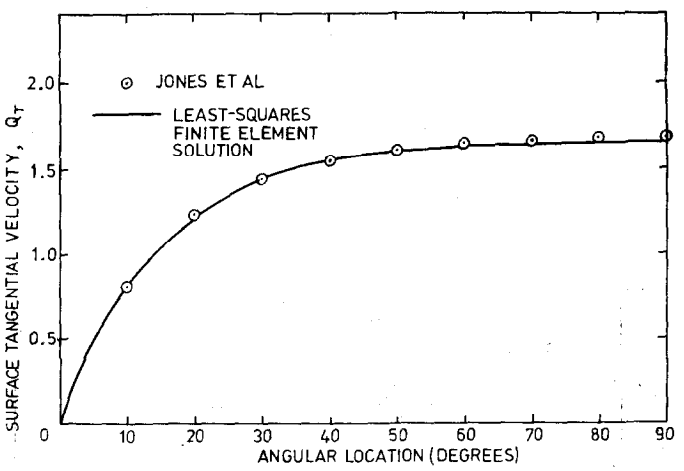

FIG. 3. Surface velocity variation for the flow about a 2:1 elliptic cylinder at $M_\infty = 0.50$.

and 829 nodal unknowns. The finite element solutions agree closely with solutions obtained by the method of lines [17]. For this case the numerical solutions indicated that the flow was everywhere subcritical.

Numerical solutions for the flow about a 6% circular-arc airfoil have been obtained using a computational grid of the form shown in Fig. 4. In the region outside ABCD the elements are all rectangular. This has caused some of the terms in the stiffness matrix to be zero and hence has reduced the computation time required to manipulate those terms. Numerical solutions for the surface pressure distribution at a freestream

Mach number of 0.71 are presented in Fig. 5. The finite element results were obtained with 102 elements and 868 nodal unknowns. Also shown in Fig. 5 are experimental results due to Knechtel [18]. The smooth airfoil results would have had a laminar boundary layer at least to the 50% chord point. By introducing roughness just aft of the leading edge the turbulent boundary layer extends over the whole airfoil. The close agreement between the finite element results and the experimental results for a smooth airfoil is slightly misleading. Since the computational results take no account

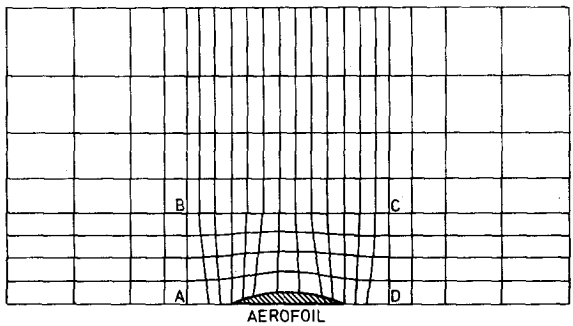

FIG. 4. Schematic of grid used for the circular-arc airfoil.

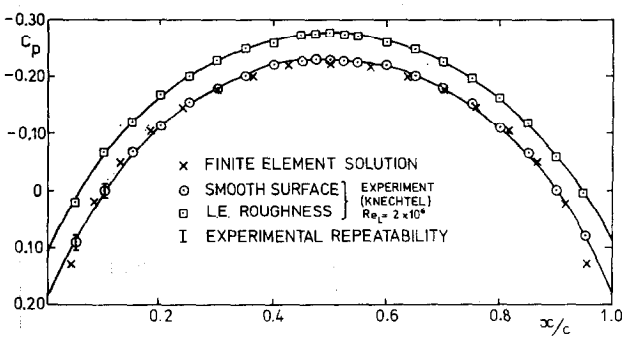

FIG. 5. Pressure distribution on a 6% circular-arc airfoil at $M_\infty = 0.71$.

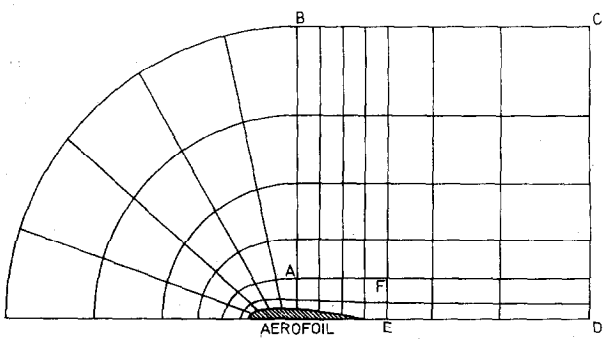

FIG. 6. Schematic of grid used for the NACA-0012 airfoil.

of the displacement effect of the viscous boundary layer the computational results would be in better agreement if they were slightly above the experimental results.

Computational results have been obtained for the flow about a NACA-0012 airfoil using a grid of the form shown in Fig. 6. The use of a polar grid adjacent to the nose of the airfoil permits more nodes to be placed in the region where the nodal unknowns vary rapidly with position. In the region ABCDEFA all the elements are rectangular. Computational results for freestream Mach numbers of 0.4 and 0.72 are shown in Figs. 7 and 8. The finite element solutions shown in Fig. 7 were obtained with 88 elements and 767 nodal unknowns. Also shown in Fig. 7 are experimental results due to Amick [19] and numerical results due to Emmons [20]. However, whereas the finite element solution corresponds to an airfoil in an undisturbed freestream, the

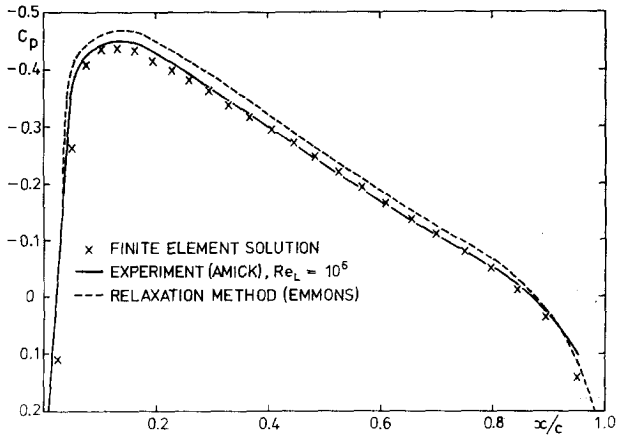

FIG. 7. Pressure distribution on an NASA-0012 airfoil at $M_\infty = 0.40$.

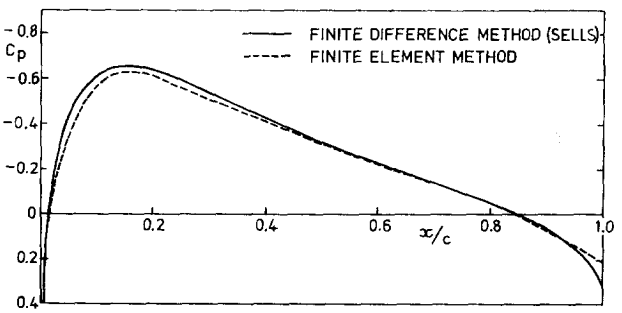

FIG. 8. Pressure distribution on an NACA-0012 airfoil at $M_\infty = 0.72$.

results of [19, 20] correspond to an airfoil in a wind tunnel. The application of a wind tunnel blockage correction to the results of [19, 20] would reduce the peak negative pressure coefficient by approximately 4 to 5%.

Finite element solutions for a freestream Mach number of 0.72 are compared with a finite difference solution due to Sells [21] in Fig. 8. The finite element results

were obtained with 96 elements and 837 nodal unknowns. Agreement is reasonable except near the nose of the airfoil, probably due to the coarseness of the grid used there.

5. Conclusion

A primitive variable, least-squares finite element formulation has been applied to inviscid, compressible flow. A unique feature of the formulation is the analytic representation of groups of terms rather than individual terms. Numerical solutions of high accuracy have been obtained for two-dimensional subcritical flow. A generalization of the least-squares method to permit the proper treatment of flows for which isolated shock waves and regions of supersonic flow occur is currently under investigation.

APPENDIX: Derivation of the Algebraic Equations Obtained from the Least-Squares Formulation

After application of the least-squares finite element formulation to Eqs. (4)–(6), the following algebraic equations are obtained

$$S_i^{(m)} = \sum_j \{r_{ij}^{(m)} \cdot (\overline{\rho u})_j + s_{ij}^{(m)} \cdot (\overline{\rho v})_j + t_{ij}^{(m)} \cdot (\overline{\rho u^2})_j + x_{ij}^{(m)} \cdot (\overline{\rho uv})_j + y_{ij}^{(m)} \cdot (\overline{\rho v^2})_j + z_{ij}^{(m)} \cdot \bar{p}_j\} = 0, \qquad m = 1, 3, \quad i = 1, n.$$

In the following expressions for $r_{ij}^{(m)}$, etc., a_{ij}, b_{ij}, c_{ij}, d_{ij} are defined by Eqs. (20)

$$\begin{aligned}
r_{ij}^{(1)} &= \alpha_c \cdot a_{ij} \cdot \bar{\rho}_i, \\
s_{ij}^{(1)} &= \alpha_c \cdot c_{ij} \cdot \bar{\rho}_i, \\
t_{ij}^{(1)} &= \alpha_x \cdot \{2 \cdot a_{ij} \cdot (\overline{\rho u})_i + d_{ij} \cdot (\overline{\rho v})_i\}, \\
x_{ij}^{(1)} &= \alpha_y \cdot c_{ij} \cdot (\overline{\rho v})_i, \\
y_{ij}^{(1)} &= \alpha_x \cdot \{2 \cdot c_{ij} \cdot (\overline{\rho u})_i + b_{ij} \cdot (\overline{\rho v})_i\} + \alpha_y \cdot a_{ij} \cdot (\overline{\rho v})_i, \\
z_{ij}^{(1)} &= \alpha_x \cdot \{2 \cdot a_{ij} \cdot (\overline{\rho u})_i + d_{ij} \cdot (\overline{\rho v})_i\} + \alpha_y \cdot c_{ij} \cdot (\overline{\rho v})_i.
\end{aligned}$$

$$\begin{aligned}
r_{ij}^{(2)} &= \alpha_c \cdot d_{ij} \cdot \bar{\rho}_i, \\
s_{ij}^{(2)} &= \alpha_c \cdot b_{ij} \cdot \bar{\rho}_i, \\
t_{ij}^{(2)} &= \alpha_x \cdot d_{ij} \cdot (\overline{\rho u})_i, \\
x_{ij}^{(2)} &= \alpha_y \cdot \{c_{ij} \cdot (\overline{\rho u})_i + 2 \cdot b_{ij} \cdot (\overline{\rho v})_i\}, \\
y_{ij}^{(2)} &= \alpha_x \cdot b_{ij} \cdot (\overline{\rho u})_i + \alpha_y \{a_{ij} \cdot (\overline{\rho u})_i + 2 \cdot d_{ij} \cdot (\overline{\rho v})_i\}, \\
z_{ij}^{(2)} &= \alpha_x \cdot d_{ij} \cdot (\overline{\rho u})_i + \alpha_y \{c_{ij} \cdot (\overline{\rho u})_i + 2 \cdot b_{ij} \cdot (\overline{\rho v})_i\}.
\end{aligned}$$

$$r_{ij}^{(3)} = 0,$$

$$s_{ij}^{(3)} = 0,$$

$$t_{ij}^{(3)} = \alpha_x \cdot \{a_{ij} \cdot \overline{rmu} - d_{ij} \cdot (\overline{\rho u})_i \cdot (\overline{\rho v})_i\},$$

$$x_{ij}^{(3)} = \alpha_y \cdot \{b_{ij} \cdot \overline{rmv} - c_{ij} \cdot (\overline{\rho u})_i \cdot (\overline{\rho v})_i\},$$

$$y_{ij}^{(3)} = \alpha_x \cdot \{c_{ij} \cdot \overline{rmu} - b_{ij} \cdot (\overline{\rho u})_i \cdot (\overline{\rho v})_i\} + \alpha_y \cdot \{d_{ij} \cdot \overline{rmv} - a_{ij} \cdot (\overline{\rho u})_i \cdot (\overline{\rho v})_i\},$$

$$z_{ij}^{(3)} = \alpha_x \cdot \{a_{ij} \cdot \overline{rmu} - d_{ij} \cdot (\overline{\rho u})_i \cdot (\overline{\rho v})_i\} + \alpha_y \cdot \{b_{ij} \cdot \overline{rmv} - c_{ij} \cdot (\overline{\rho u})_i \cdot (\overline{\rho v})_i\},$$

where $\overline{rmu} = \bar{\rho}_i^{\gamma+1}/M_\infty{}^2 - (\overline{\rho u})_i^2$ and $\overline{rmv} = \bar{\rho}_i^{\gamma+1}/M_\infty{}^2 - (\overline{\rho v})_i^2$.

REFERENCES

1. R. T. CHENG, *Phys. Fluids* **15** (1972), 2098–2105.
2. R. I. TANNER, R. E. NICKELL, AND R. W. BILGER, *Commun. Meth. Appl. Mech. Eng.* **6** (1975), 155–174.
3. M. KAWAHARA, N. YOSHIMURA, AND K. NAKAGAWA, *Int. J. Num. Meth. Eng.* **10** (1976), 437–456.
4. G. DEVRIES AND D. H. NORRIE, *J. Appl. Mech.* **38** (1971), 798–802.
5. J. PERIAUX, *Int. J. Num. Meth. Eng.* **9** (1975), 775–833.
6. TH. E. LABRUJERE AND J. VAN DER VOOREN, "Finite Element Calculation of Axisymmetric Subcritical, Compressible Flow," TR-74162U, National Aerospace Laboratory, The Netherland, 1974.
7. G. F. CAREY, *Commun. Meth. Appl. Mech. Eng.* **13** (1978), 129–140.
8. C. A. J. FLETCHER, "Subsonic, Inviscid Flow by the Finite Element Method," TR-1858(W), Weapons Research Establishment, South Australia, 1977.
9. C. A. J. FLETCHER AND M. HOLT, *J. Computational Physics* **18** (1975), 154–164.
10. C. A. J. FLETCHER AND M. HOLT, *J. Fluid Mech.* **74** (1976), 561–591.
11. B. SWARTZ AND B. WENDROFF, *Math. Comp.* **23** (1969), 37–49.
12. M. D. OLSON AND S. Y. TUANN, Primitive variables versus stream function finite element solutions of the Navier–Stokes equations," Proc. 2nd Internat. Symp. F.E.M., St. Margherita, 1976.
13. C. A. J. FLETCHER, "The Application of the Finite Element Method to Two-Dimensional Inviscid Flow," TN-1606 (WR & D), Weapons Research Establishment, South Australia, 1976.
14. W. C. RHEINBOLDT, "On the Solution of Large, Sparse Sets of Nonlinear Equations," TR-324, University of Maryland, 1974.
15. I. IMAI, *Proc. Phys. Math. Soc. Japan Ser. 3* **23** (1941), 180–193.
16. P. E. LUSH AND T. M. CHERRY, *J. Mech. Appl. Math.* **9** (1956), 6–21.
17. D. J. JONES, J. C. SOUTH, AND E. B. KLUNKER, *J. Computational Physics* **9** (1972), 496–527.
18. E. D. KNECHTEL, "Experimental Investigation at Transonic Speeds of Pressure Distribution over Wedge and Circular-Arc Airfoil Sections and Evaluations of Perforated Wall Interference," NASA TN-D-15, 1959.
19. J. L. AMICK, "Comparison of the Experimental Pressure Distribution on an NACA-0012 Profile at High Speeds with that Calculated by the Relaxation Method," NACA TN-2174, 1950.
20. H. W. EMMONS, "Flow of a Compressible Fluid Past a Symmetrical Airfoil in a Wind Tunnel and in Free Air," NACA TN-1746, 1948.
21. C. C. L. SELLS, "Plane, Subcritical Flow Past a Lifting Aerofoil," R.A.E. TR-67146, 1967.